5. Calibration & Monitoring

Spaceborne spectral measurements over long time periods require to translate the measured signals into physical quantities and to maintain this process with high precision. Therefore calibration and monitoring of the instrument is a crucial prerequisite for any successful retrieval of atmospheric geophysical parameters.

5.1 The General Calibration Equation

The goal of the calibration is to convert electronic signals of detectors (Binary Units – BU) into physical units (e.g. W/m^2/nm). This is achieved by applying a complex sequence of individual calibration steps to measurement data (for a detailed description of each step see *Slijkhuis 2000a* and *Lichtenberg et al. 2005*). The general calibration formula for any spectrometer is (equ. 5-1)

$$S_{det} = I(\lambda) \cdot \Gamma_{inst}(\lambda) \cdot QE(T_{det}, \lambda) + S_{stray} + DC + S_{elec}$$

where S_D is the signal measured on the detector, I the incoming intensity, Γ_{inst} the total transmission of the instrument, QE the detector temperature dependent quantum efficiency, S_{stray} the stray light, DC the total dark signal and S_{elec} electronic effects such as non-linearity. This equation must be solved for every detector pixel. In order to obtain the spectrum as a function of wavelength λ for each pixel, the wavelength has to be determined and the equation has to be inverted to calculate the intensity I. Generally, the transmission of the instrument is dependent on the polarisation of the incoming light.

The experience gained from GOME flying onboard the ERS-2 satellite, where various air-vacuum effects led to calibration problems, showed that spectrometers should ideally be calibrated under thermal vacuum conditions. In the case of SCIAMACHY a range of incidence angles on the mirror(s) and mirror-diffuser combinations had to be covered in the calibration, requiring a rotation of the instrument. The available vacuum tank was too small to allow a sufficiently large rotation. Therefore, a combination of TV and ambient measurements was used. The radiometric sensitivity and the polarisation sensitivity of the instrument were measured under TV conditions for *one* reference angle α_0 and all necessary instrument modes (limb, nadir and irradiance). In order to

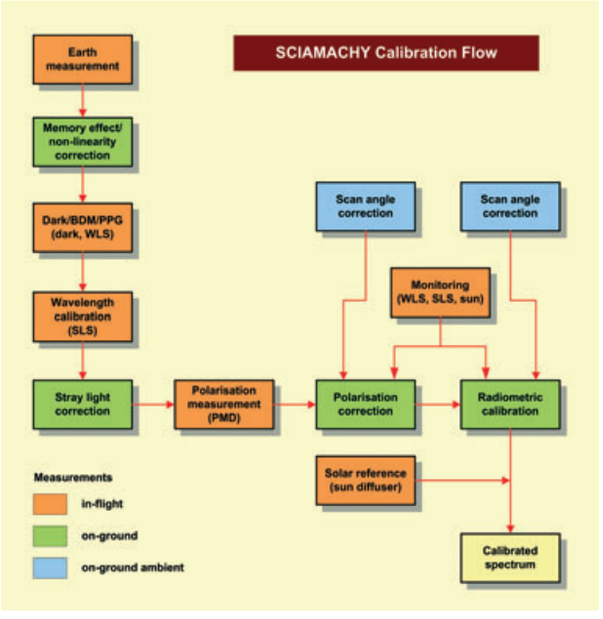

Fig. 5-1: Calibration concept for SCIAMACHY. The final calibrated Earth radiance spectra are obtained by applying several calibration steps to the measured Earthshine signals. They include in-flight calibration measurements (red), on-ground measurements performed under thermal vacuum conditions (green) and component measurements from on-ground ambient tests (blue). The optical performance monitoring (red) provides additional corrections. (graphics: SRON)

be able to calibrate all incidence angles on the mirrors (or diffusers), component level measurements of all possible mirror combinations and the mirror/ESM diffuser combination were made under ambient conditions. The detectors used in the ambient calibration were different from the detectors used on-board SCIAMACHY. These ambient measurements occurred for a set of angles – including the reference angle measured under TV conditions – and a set of selected wavelengths. From such ambient measurements the so-called *scan-angle correction* is calculated. The reference angle measurement is used to transfer the results from the ambient measurement to the TV conditions. Measurements included unpolarised light, s- and p-polarised light and ±45° polarised light. Combining TV measurements with the ambient measurements gives ideally the correct instrument response for all incidence angles at Begin-of-Life (BOL) of the instrument. The implicit assumptions for the combination of the TV and ambient measurements are that the polarisation dependence of the mirrors and diffusers are the same in air and in vacuum and that there is no temperature dependence. Both assumptions are reasonable for

SCIAMACHY, since uncoated mirrors are used. Critical points in the transfer of ambient and TV measurements are the geometry (incidence angles on the mirrors or diffusers), the illumination conditions and the detector used for the component measurements. Obviously, errors in the geometry lead to an incorrect angle dependence for the calibration quantity to be measured. Light levels during instrument measurements and during component measurements will always be different. While the footprint of the light source on the component can be matched to the footprint during the instrument measurements, it is impossible to recreate the exact illumination conditions. This may introduce systematic errors into the calibration. Finally, care has to be taken that the detector from the measurements under ambient conditions does not introduce artefacts. In order to minimise potential errors from the measurements performed under ambient conditions, only ratios of measurements were used for the calibration where possible. The individual calibration parameters derived from the on-ground measurements are combined into a set of data files, the so-called *Key Data* files. These Key Data are applied by the data processor to derive calibrated spectra (see chapter 8).

The TV on-ground calibration was performed during several campaigns using the OPTEC facility. SCIAMACHY had been placed inside the vacuum chamber with the thermal hardware being replaced by a system based on liquid nitrogen and heaters to reach and maintain the correct temperature. Optical windows in the tank allowed the light from external optical stimuli to enter. In the Key Data the effect of the optical window has been compensated for. The OPTEC facility was first used for requirement verification tests, i.e. a check to see if the instrument met its requirements. Later, calibration measurements were performed in OPTEC. Mainly due to major hardware changes in the instrument, several OPTEC campaigns had to be scheduled and executed. After the OPTEC-1 campaign it was discovered that the mounting of the optics was unreliable at low temperatures. The refurbishment implied a re-testing, and thus an OPTEC-2 campaign. Here it was found that the SWIR channels 7 & 8 were out of focus so that the OPTEC-3 campaign, executed after repositioning of channels 7 & 8, verified the required performance. In the OPTEC-4 campaign the instrument was relocated inside the facility to get representative illumination for the on-board diffuser. This configuration yielded improved measurements quantifying the instrument's radiometric properties. Finally, the stray light in the UV channels was reduced by some hardware changes which required the OPTEC-5 campaign. In all, the various OPTEC campaigns ran from summer 1997 till spring 2000.

The ambient calibration was executed between December 1997 and April 1998 in a dedicated set-up, the so-called ARCF (Absolute Radiometric Calibration Facility). In order to allow a rotation of the mirror(s) or the mirror/diffuser combination to any required position, they were placed on a special optical bench. Having two mirrors or a mirror plus a diffuser on the optical bench permitted direct measurement of the combined response of both optical elements and calibration of all SCIAMACHY instrument modes at the appropriate angles. A monochromator and polarisers were used to obtain the response for different wavelengths and polarisations. All measurements took place in a class 100 cleanroom with a controlled temperature of 20 °C and 50% air humidity.

5.2 Detector Corrections

Several corrections related to the electronics of the detectors and the detectors themselves, i.e. the terms S_{elec} and *DC* in equ. 5-1 have to be applied (see fig. 5-1). The UV-VIS-NIR channels 1-5 and the SWIR channels 6-8 must be treated separately during the calibration due to their different detector material and readout electronics. Signals are described in terms of Binary Units. The Analogue-to-Digital Converter (ADC) of SCIAMACHY digitises the signal of the detector with 16 bit resolution, meaning that detector signals (referred to as 'fillings') range from 0 BU to 65535 BU.

Channels 1-5 (UV-VIS-NIR)

The first correction to the data is the so-called *Memory* effect. The Memory effect was discovered in 1996 during an investigation of the linearity of channels 1-5. In a number of measurements covering the range from low detector fillings to saturation it was found that the signal deviated from a linear response which is defined by a linear fit for all points of up to 90% of the maximum detector fillings (fig. 5-2). The deviation was independent of the actual signal level, but dependent on the signal level of the *previous* readout (hence the name *Memory* effect). Note that the effect depends on the signal level *including* the analogue offset (see below) and dark current. Thus it has to be applied before any other correction. In order to characterise the Memory effect, WLS measurements followed by several dark measurements were performed on-ground and in-flight. The difference between the first dark measurement after the WLS measurement and subsequent dark measurements gives a correc-

tion value as a function of detector filling. This value needs to be subtracted from the data to correct for the Memory effect which is the same for all pixels. The total correction for a single readout amounts from -0.61% to 0.21% of the detector filling of the previous readout with a maximum effect at fillings around 19 000-21 000 BU, depending on the channel. More information can be found in *(Lichtenberg 2003)*.

The second detector correction to be applied is the dark signal correction. The dark signal is measured in every orbit during eclipse using 5 different states. In channels 1-5 the dark signal consists of two components: the analogue offset (AO) and the leakage current (LC). The analogue offset is independent of time, it is just a fixed signal added to the measured signal to avoid negative signals. The leakage current is caused by thermally created electron-hole pairs. The total dark signal for channels 1-5 is (equ. 5-2)

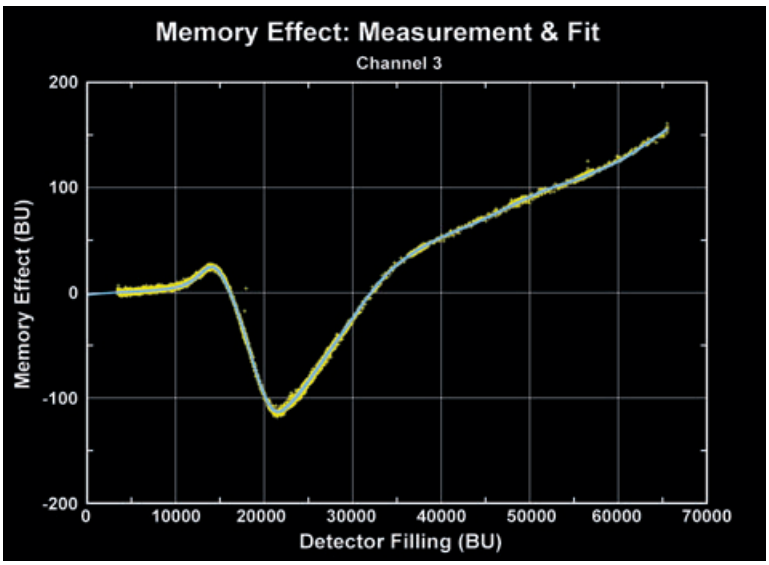

Fig. 5-2: Memory effect for channel 3. Yellow crosses mark the in-flight measurement of the Memory effect. The blue solid line is a spline fit through the measurements that is used for the correction. (graphics: SRON)

$$DC_{ch15} = f_{coadd} \cdot AO + f_{coadd} \cdot t_{PET} \cdot LC$$

where f_{coadd} and t_{PET} are the co-adding factor of the cluster and the pixel exposure time, respectively. Note that the analogue offset is only multiplied with the co-adding factor since it is not dependent on the integration time and is added to the signal for every detector readout. Linear fitting to dark measurements with different integration times yields the in-flight dark signal correction. The dark signal in the UV-VIS-NIR channels is dominated by the analogue offset while the leakage current amounts to only 0.04-0.5 BU/sec and has not changed significantly since launch.

Channels 6-8 (SWIR)

The SWIR channels do not suffer from the Memory effect. However, these channels display a significant non-linearity, i.e. a deviation in the detector response from a (chosen) linear curve. The non-linearity has been measured during the on-ground calibration campaign and a correction algorithm was defined. The maximum value of the non-linearity is around 250 BU which can be significant for weak absorbers such as CO. A separate non-linearity correction for the channels 6, 6+, 7 and 8 has been derived. Within these channels the non-linearity differs for odd and even pixels (starting pixel numbering with 0) because of the different multiplexers used for odd and even pixels. Additionally, there is a clear difference in the non-linearity between pixel numbers higher and lower than pixel number 511. This leads to 14 correction curves, four per channel with the exception of channel 6+, which covers only pixels 794 to 1024. Fig. 5-3 shows the non-linearity curves derived for channel 8. The accuracy of the non-linearity correction corresponds to 5-21 BU for detector fillings from 10 000-40 000 BU, depending on the channel. As for the Memory effect correction, the non-linearity has to be corrected before any other correction is applied. More details about the non-linearity can be found in *(Kleipool 2003)*.

In addition to the non-linearity, channels 6+, 7 and 8 contain a significant number of unusable pixels due to the lattice mismatch between the light detecting InGaAs layer and the InP substrate. These channels are doted with a higher amount of Indium (see chapter 3). It changes the lattice constant of the light detecting layer so that it no longer matches the lattice constant of the substrate on which the detecting layer is grown. The resulting degraded pixels are called 'bad' or 'dead' pixels. There are various effects making these pixels unusable:

- disconnected pixels preventing any signal readout
- so-called Random Telegraph (RT) pixels which spontaneously and unpredictably jump between two levels of dark current leading to different detected signals for the same intensity
- other effects including excessive noise or too high leakage current that saturates the detector

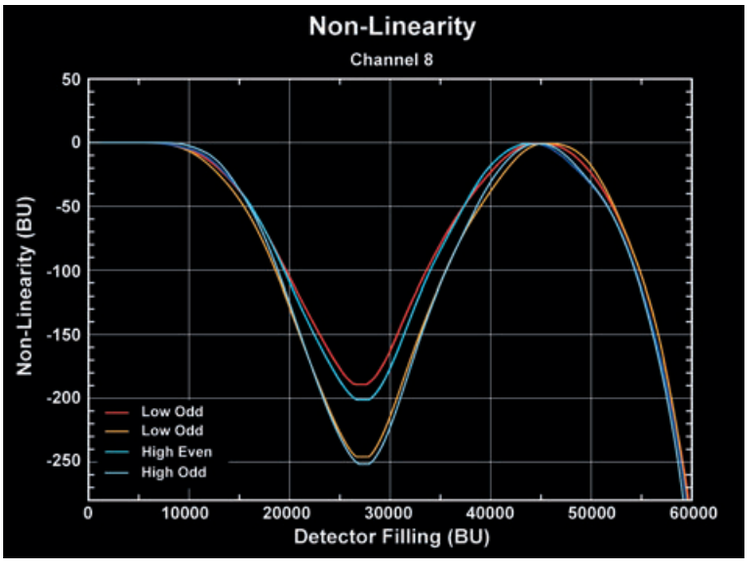

Fig. 5-3: Non-Linearity in channel 8 for different pixel regions (indicated by colours). 'Low' pixels are those with pixel numbers below 512. The pixel numbering starts at 0. (graphics: SRON)

All these effects were measured on-ground and a Bad and Dead Pixel Mask (BDM) was created. Pixels of the BDM have to be ignored in any retrieval.

After the application of the non-linearity and the BDM, the dark signal has to be corrected. The dark signal correction in channels 7 and 8 is complicated by the presence of a large thermal background BG_{th} and the unforeseen growth of an ice layer on the detector (see chapter 6.3). The ice layer slowly changes the detector temperature and attenuates the signal on the detector, including the thermal background. The dark signal in these channels becomes (equ. 5-3)

$$DC_{ch68} = f_{coadd} \cdot \left(AO + t_{PET} \cdot LC + t_{PET} \cdot \Gamma_{ice} \cdot QE(T_{det}, \lambda) \cdot BG_{th}(\varphi)\right)$$

where Γ_{ice} is the transmission coefficient that changes due to the ice layer and QE is the quantum efficiency for the detector.

For channels 6+ and 8 the quantum efficiency changes with the detector temperature T_{det}, whereas the first part of channel 6 and 7 shows no significant temperature dependence. The thermal background is caused by the thermal radiation of the instrument and is the dominant part of the dark signal (about 4000 BU/sec) in channel 8. It depends on the orbit phase φ because the temperature of the instrument is not completely stable but varies over one orbit due to the changing angle of solar irradiation. The variation of the dark signal over the orbit can reach up to 60 BU/sec which has significant impact on the retrievals of trace gases. In-flight the orbital variation is measured once a month during a special calibration orbit in which only dark signal measurements are performed by looking to deep space at a tangent height of 250 km in limb mode. The variation of the transmission makes the dark signal correction time dependent meaning that for channels 7 and 8 a dark signal correction, calculated from measurements in the same orbit, must be used.

The final detector related correction is the Pixel-to-Pixel Gain (PPG) correction. The pixels in the SWIR channels do not show the same response to incoming light. Variations of a few percent can be observed. The PPG is derived by first smoothing a WLS measurement, assuming the spectrum is flat. Then the original spectrum is divided by the smoothed measurement, leaving only the high frequent variations that are caused by the different pixel gains in the result. The PPG is strictly an effect caused by the electronics and the detector and is thus associated to the individual pixels but not to the wavelength.

5.3 Wavelength Calibration

In-flight spectral calibration of SCIAMACHY data uses the internal SLS measurements with the exception of channels 7 and 8 (see below). For selected lines the Falk algorithm *(Falk 1984)* determines the pixel positions. These are then fitted to theoretical line positions provided with the calibration data. From the polynomial coefficients of the fit the wavelength for each pixel can be calculated. Measurements of solar Fraunhofer lines serve as a quality check. In channels 7 and 8 a calibration with the internal SLS lamp is impossible because in these channels not enough useful lines are available to calculate the wavelength calibration with sufficient accuracy. In channel 8 this is caused by bad pixels interfering with the determination of the line position. Channel 7 only contains two strong doublet lines preventing an accurate determination of line positions over the whole channel. In both channels data from on-ground gas cell absorption measurements establish the wavelength calibration.

An additional effect discovered during the on-ground calibration is the so-called *Blocking Shift*: During the spectral calibration on-ground, the internal SLS and an external SLS were used. A comparison of the measurements done with the two lamps revealed a wavelength shift of up to 0.07 nm. The reason is a partial blocking of the light path during

internal SLS measurements. The blocking shift was characterised and is part of the calibration data. Verification of the spectral calibration in-flight has proven that SCIAMACHY is spectrally very stable.

5.4 Stray Light

There are two types of stray light (S_{stray} in equ. 5-1), the spectral stray light and the spatial stray light. Stray light is characterised as a fraction of the total measured intensity for a given pixel.

Spectral stray light is light of a certain wavelength which is scattered to a detector pixel 'belonging' to a different wavelength. It can lead to distortions in the shape of the spectrum. This type of stray light is usually caused by a reflection in the instrument after the dispersion of the light beam. The source of spectral stray light can be within the same channel, referred to as *intra-channel* stray light, or it can scale with the intensity in a different channel, referred to as *inter-channel* stray light.

Spatial stray light is light entering the telescope from outside the IFoV. It is dispersed just like light from the observation target. Depending on the source of the stray light, the spatial stray light component can add an additional offset to the spectrum and/or distort the spectrum, if the primary source of the stray light has spectral characteristics that differ significantly from the observed target.

Spectral Stray Light

In a full matrix approach, the spectral stray light determination would measure the stray light contribution from each individual pixel to all other pixels separately. In practice, however, this is not always possible. In the case of SCIAMACHY a 8192 × 8192 matrix would be needed making the calculation of stray light very slow. Furthermore, usually only a very small fraction of the incoming light is stray light. If the full matrix approach is used, the signal in one pixel does only produce a very weak stray light signal in the other pixels which can very well be below the measurement threshold. In order to prevent problems with the full matrix approach the spectral stray light for SCIAMACHY was separated into three types: uniform stray light, ghost stray light and channel 1 stray light.

Each type of stray light was characterised on-ground using measurements employing a monochromator. A monochromator produces light in a narrow, pre-defined spectral band. The centre wavelength of the spectral band can be adjusted. In the derivation of the stray light fractions from monochromator measurements it is assumed that any signal in detector pixels outside this spectral band is caused by stray light. During the on-ground calibration the spectral stray light was measured by changing the central wavelength of the monochromator spectral band, thus covering the whole wavelength range of SCIAMACHY. Dividing the integrated light of the monochromator peak(s) by the light detected outside the peak yielded the stray light fraction. The resulting data is part of the calibration data set and is used to correct the spectral stray light in-flight.

The uniform stray light is caused by a diffuse reflection which adds some signal to all detector pixels in a given channel. Being independent of wavelength, the uniform stray light fraction in channels 2-8 is between 0.07% and 0.1% of the average signal on the detector, depending on the channel. Its relative error as determined during the on-ground calibration ranges between 15% and 40% of the calculated value, again depending on the channel. Even with the maximum error, the largest expected stray light fraction amounts to 0.14% only, which is well within the requirements. It is assumed that the uniform stray light does not depend on polarisation.

Ghost stray light is caused by a more or less focused reflection of one part of a spectrum to another part of the spectrum. It can distort the shape of the 'true' spectrum, because it does not add signal to all pixels. During the on-ground measurements 15 ghost signals were detected in channels 2-8. The total sum of ghost stray light in a channel is at maximum 1% of the incoming intensity.

For channel 1 the situation is less favourable with respect to stray light levels. The on-ground measurements revealed that the spectral stray light in channel 1 can reach levels of up to 10% of the incoming signal for a typical input spectrum. It is also highly wavelength dependent. The main reason for the larger stray light fraction in channel 1 is the high dynamic range of the spectra in this channel, with the lowest signal 3 orders of magnitude smaller than the highest signal. The coarse, artificial separation in uniform and ghost stray light turned out to be insufficient for a correction in channel 1 and an alternative method had to be formulated. The chosen approach combines the correction of uniform and ghost stray light in a modified matrix approach. In order to avoid signal-to-noise problems during the spectral stray light measurements, ten wavelength bands were defined separately for s- and p-polarised light leading to a total of 20 bands. For both polarisation directions 9 bands were located in channel 1 to characterise intra-channel stray light and one band covered the signal from channels 2-5 to characterise inter-

channel stray light. The channel 1 detector material is not sensitive for light with wavelengths longer than 1000 nm so the SWIR channels did not need to be considered. For each band the stray light contribution to all detector pixels was calculated leading to a 10 × 1024 matrix for both, s- and p-polarised light. The stray light fraction in channel 1 ranges from less than 1% to as much as 10%. The correction has an accuracy of around 25% and reduces the stray light by an order of magnitude leaving at most 1% stray light in the spectrum after correction.

Spatial Stray Light

Shortly after ENVISAT emerges from eclipse and passes the North Pole, the sun shines directly into the limb port. In this orbit region spatial stray light cannot be avoided, i.e. the particular effect was foreseen and the data are flagged accordingly. In order to minimise spatial stray light, the ASM is rotated such that the edge of the mirror/diffuser plate points into flight direction, with the diffuser looking to the instrument side during all measurements using the ESM only. Shortly after launch it became clear however that limb measurements still suffer from a certain amount of this type of stray light with an impact on instrument in-orbit performance (see chapter 6.3 for details).

5.5 Polarisation

SCIAMACHY is – as all grating spectrometers without a polarisation scrambler – sensitive to the polarisation of the incoming light, i.e. the response will not only depend on the intensity but also on the polarisation of the light. Thus polarisation correction is required. It uses the Mueller matrix approach (see e.g. *Azzam and Bashara 1977*, *Coulson 1988*). Measurements of polarised light can be expressed by a so-called *Mueller matrix* M and the Stokes vector *S* (equ. 5-4):

$$S_{det} = \mathrm{M} \cdot S_0$$

This yields (equ. 5-5):

$$\begin{pmatrix} S \\ Q \\ U \end{pmatrix}_{det} = \begin{pmatrix} M_{11} & M_{12} & M_{13} \\ M_{21} & M_{22} & M_{23} \\ M_{31} & M_{32} & M_{33} \end{pmatrix} \cdot \begin{pmatrix} I \\ Q \\ U \end{pmatrix}_0$$

where on the left hand side of the equation a Stokes vector describes the light as detected by the instrument, i.e. in front of the detectors, and on the right hand side we have the Mueller matrix defining the response of the instrument to the incoming light represented by another Stokes vector. The first element of this Stokes vector, *I*, denotes the total intensity of the light (we use *S* for the detected signal on the left hand side of the equation). *Q* is a measure for the polarisation along the x- or y-axis of a chosen reference frame and can be described as $Q = I_x - I_y$. *U* is a measure for the polarisation along the 45° direction and is defined as $U = I_{45} - I_{-45}$. Note that the total intensity can be written as $I = I_x + I_y$ or $I = I_{45} + I_{-45}$. Often *Q* and *U* are normalised to the total intensity *I*. We will denote normalised fractions with *q* and *u*.

The formula given above is only correct for Earth observations where the circular polarisation of the light *V* can be neglected. This is usually the case and thus circular polarisation is not considered in the polarisation correction. All Mueller matrix elements are dependent on wavelength and on the incidence angle of the light on the scan mirror(s) or diffuser. In the calibration, ambient measurements on component level and instrument TV measurements have to be combined meaning that the actual instrument matrix has to be calculated by a multiplication of the matrix for the scanner (combination) and the OBM.

The detectors of SCIAMACHY are only sensitive to the intensity, reducing equ. 5-5 to (equ. 5-6)

$$S_{det} = M_{11}^{D,P} \cdot I \cdot \left(1 + \frac{M_{12}^{D,P}}{M_{11}^{D,P}} \cdot q + \frac{M_{13}^{D,P}}{M_{11}^{D,P}} \cdot u\right)$$

$M_{11}^{D,P}$ is the radiometric sensitivity of the instrument ('*D*' = detector, '*P*' = PMD). The term in brackets is the inverse of the polarisation correction factor, c_{pol}. It depends on the polarisation sensitivity of the instrument – represented by the ratios of matrix elements – and the polarisation of the incoming light *q* and *u*. The problem of correcting the response of the instrument for polarisation can thus be divided into two parts: (1) determining the polarisation sensitivity of the instrument and (2) determining the polarisation of the incoming light during the science measurements in-flight. The polarisation sensitivity was measured on-ground using ratios of measurements as far as possible to minimise influences of the measurement setup on the data. The polarisation reference frame used in the calibration is defined w.r.t. the direction of the slit: looking in the direction of the light entering the instrument after the scan mirrors, the +45° polarisation direction is obtained by a 45° clockwise rotation from the p-polarisation direction. The p-polarisation direction is aligned with the long

side of the entrance slit of SCIAMACHY. All calibration data use this reference frame. SCIAMACHY exhibits a different sensitivity to s- and p-polarised light and to +45° and -45° polarised light. Thus, in the on-ground calibration, measurements with fully s-, p-, +45° and -45° polarised light in ambient and under thermal vacuum conditions are used to derive η, the s/p sensitivity of SCIAMACHY and ζ, the -45°/+45° sensitivity for the limb and the nadir configuration. Care was taken to ensure that the intensity in all these measurements was the same. The polarisation correction factor in terms of on-ground measurements is with the definitions given above (equ. 5-7)

$$c_{pol} = \left(1 + \frac{1-\eta}{1+\eta} \cdot q + \frac{1-\zeta}{1+\zeta} \cdot u\right)^{-1}$$

The second step, the determination of the polarisation of the incoming light is done by determining the ratio of the signal in the PMD channels – which is fully polarised due to the Brewster reflection at the pre-disperser prism (see chapter 3.2) – and the corresponding signal in the science channel for each individual measurement. During calibration this ratio was determined for s-, p-, +45° and -45° polarised light. The comparison of the in-flight ratio with the calibration data gives 7 polarisation values for the whole spectrum, one for each PMD channel. Polarisation values q are calculated from PMD A-F needing the corresponding value of u. The ratio u/q, which depends only on the polarisation angle, is assumed to be constant, such that (equ. 5-8)

$$u_{measured} = q_{measured} \cdot (u/q)_{const}$$

In the original calibration concept, for UV-VIS wavelengths below 600 nm the polarisation angle from single scattering theory was planned to be used (see below), whereas for higher wavelengths the ratio u/q from PMD D and PMD 45°, both centered around 850 nm, had to be taken. The values of q and u here are derived by iteration, until the u needed to calculate q from PMD D and the q needed to calculate u from PMD 45°, match. In-flight it was noted that

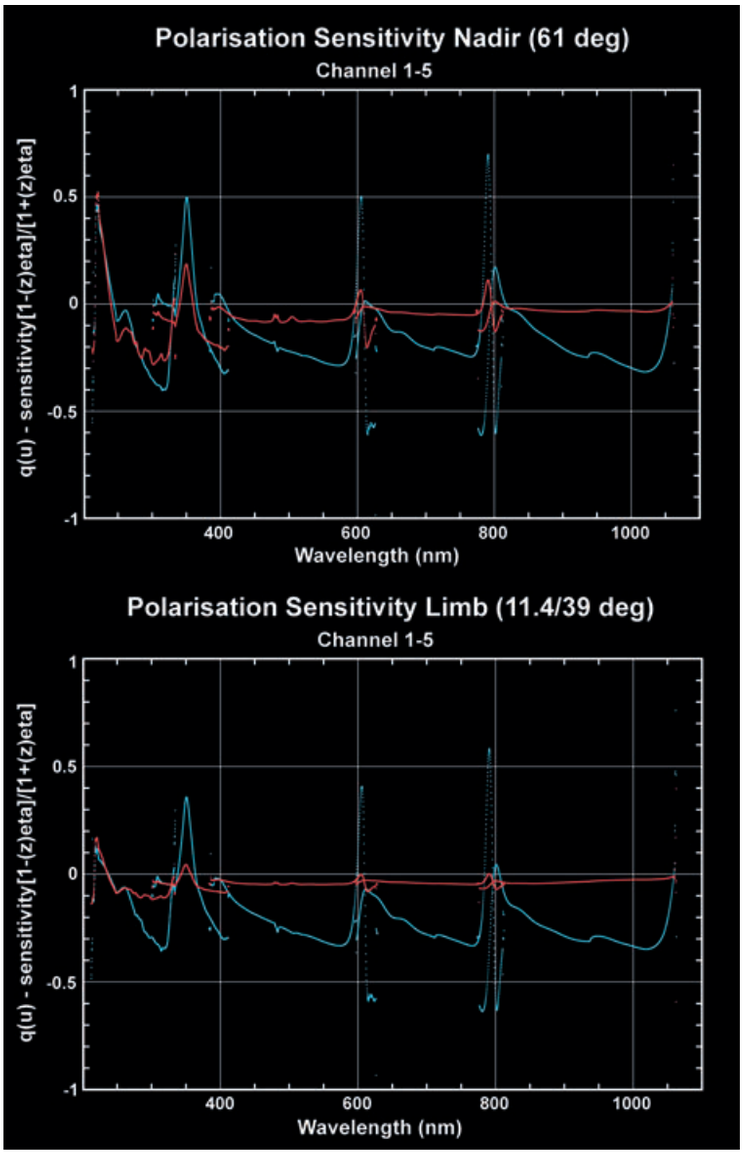

Fig. 5-4: q (blue) and u (red) sensitivity from equ. 5-6 for nadir (elevation angle of 61° top) and for limb (elevation angle of 11.4° and azimuth angle of 39°, bottom) for channels 1-5. Note that these sensitivities are multiplied with the polarisation fractions to get c_{pol} and the correction will thus be smaller than displayed for lower polarisation. (graphics: SRON)

PMD 45° delivers systematically signals which are 10-15% higher than expected, even for unpolarised sources such as the sun. As there are indications that this PMD suffers from stray light, it remains currently unused. Instead, u/q is taken from single scattering theory for the complete wavelength range. From POLDER satellite measurements of u/q this appears to be a sufficiently accurate assumption *(Schutgens et al. 2004)*. Note, that for small values of q, this ratio becomes very large, thereby amplifying small measurement errors on $q_{measured}$ into large measurement errors on $u_{measured}$. However, since the instrument is much more sensitive to q than to u, this has little impact on the radiometric calibration, even though u

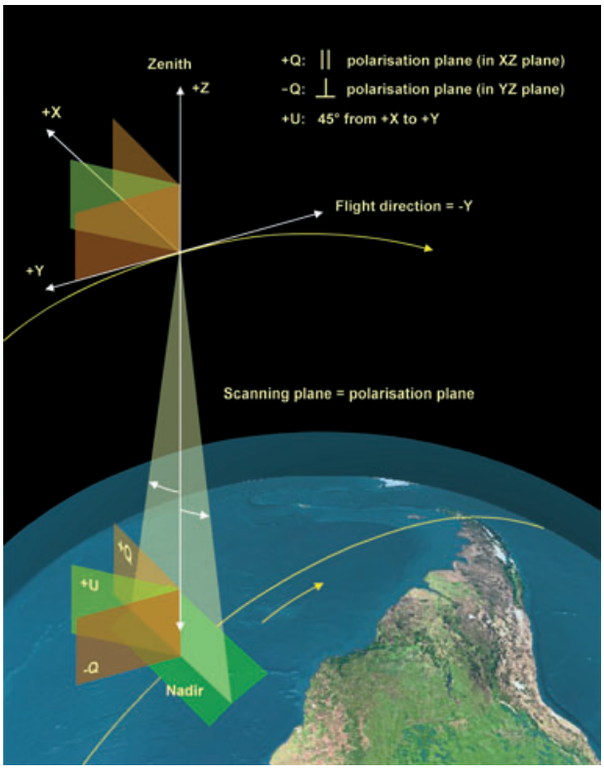

Fig. 5-5: Definition of the coordinate frame used in the data processor for polarisation values q = Q/I, u = U/I. (graphics: DLR-IMF)

is notably unreliable. In limb, the calculated polarisation displayed an unexpected drift with increasing tangent height, which is probably due to increasing significance of the spatial stray light contribution as the limb intensity decreases. Therefore the PMD measurements are only used up to 30 km. Radiative transfer calculations show that above this height the depolarisation remains constant *(Mc Linden et al. 2002)*, such that for higher limb tangent heights we are able to scale the measured polarisation at 30 km with a value obtained from single scattering theory.

The PMD channels cover only the instrument channels 2-8. For channel 1 the backscattered radiation is dominated by single scattering as can be inferred from radiative transfer calculations. Similarly to the GOME instrument, a theoretical value based on single scattering geometry is used here *(Slijkhuis 2000b, Tanzi 1999, Tilstra et al. 2003)*. The transition region from single scattering to multiple scattering and/or ground reflection in the region between approximately 300-325 nm requires special attention. For GOME, a parameterisation of the degree of polarisation as a function of wavelength was derived by R. Spurr *(Balzer et al. 1996)*, known as the 'general distribution function' (GDF) for polarisation. The GDF is characterised by the single scattering value plus three parameters. These parameters are currently obtained using a simplified version of the algorithm from *Schutgens and Stammes (2002)* where the dependence on scene albedo and ozone content is neglected. More polarisation information may be derived from the channel overlaps of channels 1-6 (five polarisation points) where the different polarisation sensitivities of each channel leads to two independent measurements for the two variables q and u. However, due to calibration inconsistencies, these polarisation points are currently not reliable.

The polarisation values q and u on the level 1b products are specified in an 'atmospheric' coordinate frame which is different from the coordinate frame used for the on-ground calibration and Key Data specification. The 'atmospheric' coordinate frame is related to the geometry of the scattering of light in the atmosphere. The choice has been to define q as parallel to the local meridian plane – the plane through satellite, zenith, and centre-of-FoV (where its Z axis points in the travel direction of light, i.e. towards the instrument). This plane is depicted in Figure 5-5 for nadir viewing geometry. For limb viewing geometry, the polarisation plane in the figure is rotated 90° as the line-of-sight is approximately in the flight direction.

5.6 Radiometric Calibration

The final step in the calibration of the data is the radiometric calibration. The retrieval of trace gases usually uses the reflectance, the ratio of Earth radiance and solar irradiance. The solar irradiance is measured with on-board diffusers in-flight. Using equ. 5-7 and equ. 5-8 the reflectance can be written as (equ. 5-9)

$$R = \frac{\pi \cdot I_{Earth}}{\mu_0 \cdot I_{sun}} = \frac{\pi \cdot S_{det}^{Earth} \cdot c_{pol}}{\mu_0 \cdot M_{11}^{N,L}} \cdot \frac{M_{11}^{sun}}{S_{det}^{sun}}$$

with $I_{Earth,Sun}$ and S_{det}^{Earth} as the Earth and sun intensity and measured signal, μ_0 as the cosine of the solar zenith angle, $M_{11}^{N,L}$ as the radiometric response for limb (L) and nadir (N) and M_{11}^{sun} as the radiometric responses for sun diffuser measurements. Because all matrix elements in equ. 5-9 relate to the detectors, we left the superscript 'D' out for better legibility. For a proper calibration the instrument responses have to be determined as a function of wavelength λ and incidence angle α. As already mentioned in chapter 5.1 the radiometric response was measured on instrument level under TV conditions and the mirror and the mirror/diffuser combination were measured under ambient conditions. In order to transfer ambient measure-

ments to TV measurements the ratio of a TV measurement to an ambient measurement at the same incidence angle, the reference angle α_0 is used (equ. 5-10)

$$C_A = \frac{R_{T/V}(\lambda)}{\eta_{OBM}(\lambda) \cdot R_s^N(\lambda,\alpha_0) + R_p^N(\lambda,\alpha_0)}$$

where $R_{T/V}$ is the radiometric response obtained under TV conditions in nadir configuration, η_{OBM} is the polarisation sensitivity of the OBM without the scan mirrors and $R_{s,p}^N$ is the reflectivity of the nadir mirror for s- and p-polarised light. Using this relation the radiometric response for Earth and sun observations can be expressed as (equ. 5-11)

$$M_{11}^{N,L}(\lambda,\alpha) = C_A \cdot \left(\eta_{OBM} \cdot R_s^{N,L}(\lambda,\alpha) + R_p^{N,L}(\lambda,\alpha)\right)$$
$$M_{11}^{sun}(\lambda,\alpha) = C_A \cdot C_N \cdot \left(\eta_{OBM} \cdot \eta_N \cdot B_s(\lambda,\alpha) + B_p(\lambda,\alpha)\right)$$

where α is the incidence angle on the mirror and diffuser, C_N corrects for the neutral density filter (NDF) located in the light path of solar measurements, η_N is the polarisation sensitivity of the NDF and $B_{s,p}$ is the reflectivity of the combination ASM mirror and ESM diffuser. The term in brackets in equ. 5-11 constitutes the above mentioned scan angle correction. The reflectance can now be derived by combining equ. 5-9, 5-10 and 5-11.

The signal from the sun can additionally be measured with the ASM diffuser/ESM mirror combination. Solar spectra obtained from ASM diffuser measurements show less spectral features than those measured with the ESM diffuser. The ASM diffuser could not be radiometrically calibrated, since it was added at a late stage after the calibration campaign. However, for DOAS like retrievals an absolute calibration is not required and ASM diffuser sun spectra can be used for these retrievals.

5.7 Optical Performance Monitoring

Contrary to system monitoring, optical performance monitoring aims at assuring an as complete as possible description of the optical performance in order to correct for degradation effects throughout the instrument's lifetime. Therefore, monitoring serves as a general prerequisite for continuous high data product quality. Monitoring related to the optical performance of SCIAMACHY is to a large degree linked to the instrument calibration & characterisation status. It establishes in-flight information which permits proper application of on-ground calibrations and modelling of the in-orbit environment.

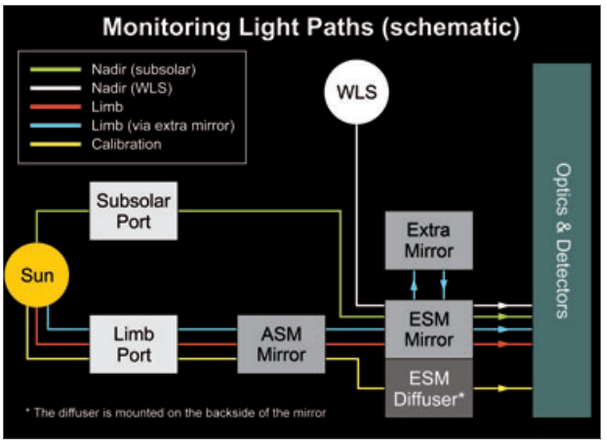

Fig. 5-6: Schematic view of SCIAMACHY light paths used in performance monitoring. (graphics: IUP-IFE, University of Bremen)

Optical component degradation monitoring is one of the main long-term monitoring activities to be performed over the mission's lifetime (*Noël et al. 2003*). It applies regular trend analyses to measurement data obtained with the internal WLS and of observations of the unobscured sun above the atmosphere. In order to monitor the different SCIAMACHY light paths, solar measurements are taken in various viewing geometries: in limb/occultation geometry (via ASM and ESM mirrors), in nadir geometry (via the ESM mirror through the sub-solar port), and via the so-called 'calibration light path' involving the ASM mirror and the ESM diffuser. Particularly the WLS produces a rather stable output over time – except for some degradation in channel 1 – which makes it well suited for throughput monitoring.

Because of the status of the operational data processing in the initial part of the mission, the monitoring of the optical performance of the SCIAMACHY instrument had to be based on the analysis of Level 0 data – which had been corrected for dead/bad pixels, dark current (fixed value from August 2002), scan angle dependencies, quantum efficiency changes and the seasonally varying distance to the sun – and not the fully calibrated level 1b spectra as originally envisaged. Due to this approach additional calibration corrections, e.g. stray light correction, were not applied. Therefore, optical throughput variations smaller than about 1% require careful investigation. However, once the light path monitoring can be based on fully calibrated data, it will yield so called *m-factors* to describe how the individual light paths degrade. These m-factors will be fed into operational data processing to ensure that the measured signals are fully matched to the performance of SCIAMACHY.

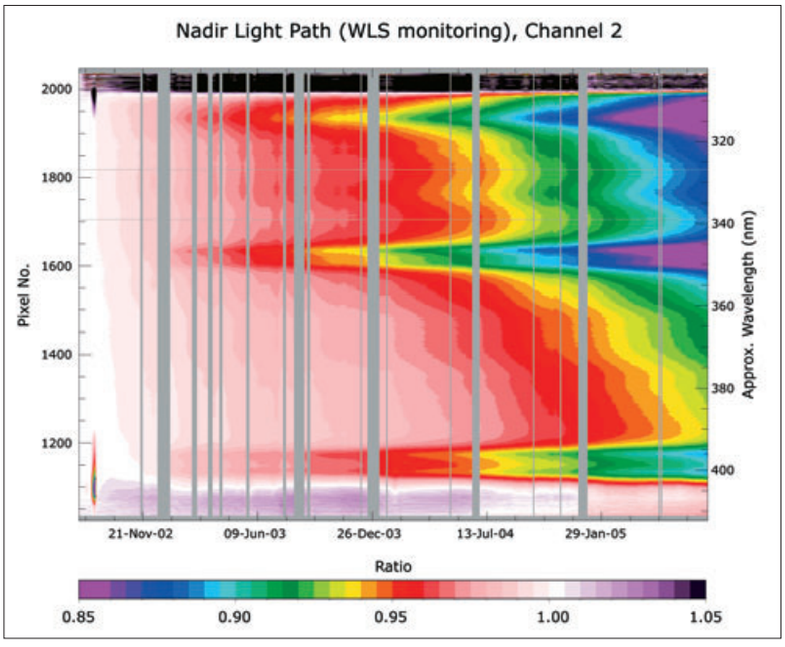

Fig. 5-7: Monitoring results for the nadir light path using measurements with the internal WLS in channel 2. All available data have been interpolated to a daily grid. (graphics: IUP-IFE, University of Bremen)

Moreover, from the combination of the results for the different light paths it will be possible to derive information about the degradation of individual optical components (mirrors and diffusers, see fig. 5-6). The degradation of the ASM mirror, for example, may be determined from the ratio of the limb to the nadir light path degradation. To determine the ESM mirror degradation it is necessary to combine the limb light path results with dedicated measurements involving the extra mirror which is located inside the instrument, only rarely used and thus assumed not to degrade. Finally, the degradation of the ESM diffuser can be computed from the combination of the nadir, limb, and calibration light path. A comparison of the limb and nadir light path monitoring results indicates that the major degrading element in the SCIAMACHY optical train seems to be the ESM mirror which shows a 3 to 4% degradation per year in the UV (channel average) which is much less than the degration of the GOME mirror.

While channel averaged optical throughputs for the first years of the mission are provided in chapter 6.3, an example for the wavelength dependence of the instrument degradation is depicted in fig. 5-7. It displays for channel 2 the relative variation of the nadir throughput – light enters the spectrometer via the ESM mirror only – as a function of time and wavelength, based on internal WLS measurements. The available measurement data have been interpolated to a daily grid. Times of reduced instrument performance (like switch-offs or decontamination periods) as well as dead/bad pixels have been masked out (gray bars). All measured signals are referenced to August 2nd, 2002, at about orbit 2200. The degradation is clearly wavelength dependent: In channel 2 (fig. 5-7) a degradation can be identified which peaks at spectral regions of high polarisation sensitivity and in the overlap regions between the channels. However, the channel 4 monitoring data presented in fig. 5-8 show the excellent absolute radiometric stability of SCIAMACHY. The degradation in this channel stays mostly within 2%, except for the channel overlaps. A similar trend can be observed in the other channels in the visible range. Spectrally dependent throughput monitoring may become an additional operational task once the operational availability of the required input products is ensured.

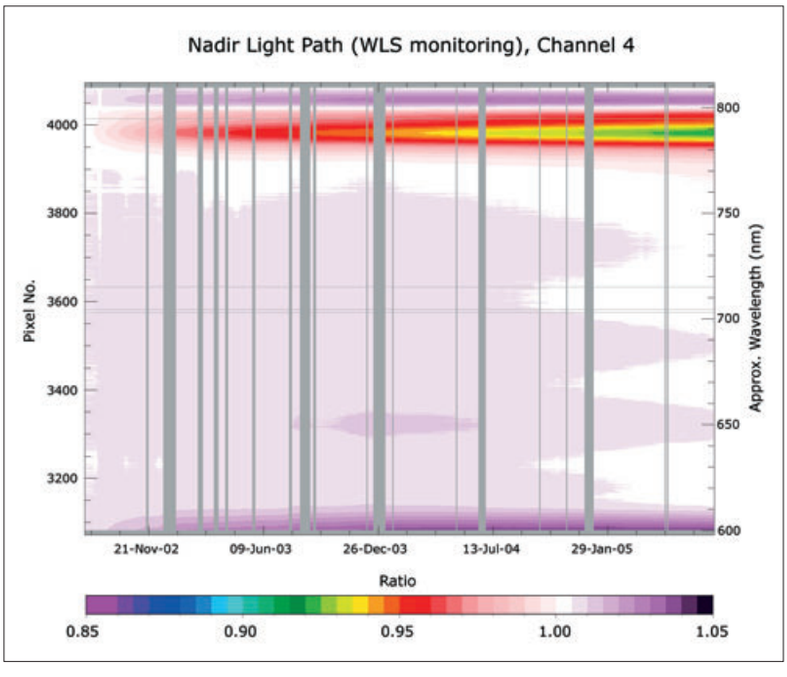

Fig. 5-8: As fig. 5-7, but results for channel 4. (graphics: IUP-IFE, University of Bremen)